Journal Name

COMMUNICATION

First-principles calculations of oxygen interstitials in corundum: site symmetry approach

0Received 00th January 20xx,
Accepted 00th January 20xx

DOI: 10.1039/x0xx00000x

www.rsc.org/

Robert A. Evarestov,[a*] Alexander Platonenko[b], Denis Gryaznov[b], Yuri F. Zhukovskii[b], and Eugene A. Kotomin[b,c]

Using the site symmetry analysis, four possible positions of interstitial oxygen atoms in α-Al_2O_3 hexagonal structure have been identified and studied. First principles hybrid functional calculations of the relevant atomic and electronic structures for interstitial O_i atom insertion in these positions reveal differences in energies ~1.5 eV. This approach allows us to get the lowest energy configuration avoiding time-consuming calculations. It is shown that the triplet oxygen atom is barrierless displaced towards the nearest regular oxygen ion, forming a siglet dumbbell (split interstitial) configuration with the energy gain of ~2.5 eV. The charge and spatial structure of the dumbbell is discussed Our results are important, in particular, for understanding the radiation properties and stability of α-Al_2O_3 and other oxide crystals.

α-Al_2O_3 (corundum, sapphire) is a promising material for future fusion reactors, e.g. for components such as breeder blanket and diagnostic windows.[1-4] Thus, this is important to understand and control its radiation damage under intensive neutron irradiation. As well known, radiation produces pairs of the Frenkel defects – interstitials and vacancies – in both cation[5-9] and anion[10-14] sublattices. Along with neutron irradiation, effects of proton[15] and heavy swift ions were studied[13]. The most studied in corundum are the electronic defects (color centers) in oxygen sublattice where the vacancies trap one or two electrons (the F^+ and F centers, respectively).[7,12-14,16] Anion-deficient crystals with carbon impurities are used as highly sensitive personal dosimeters and for environmental radiation monitoring.[17,18]

In contrast to the electron centers, properties of interstitial oxygen atoms are experimentally very poorly studied, due to lack of magnetic properties and optical absorption in a suitable energy range. Such a study is very important since in most binary oxides (as well as in alkali halides) the oxygen/halide interstitials are more mobile than complementary vacancies, and their diffusion-controlled recombination determines *stable* defect concentrations at moderate and high temperatures.[19]

Several theoretical studies from first principles were performed for the oxygen interstitials in binary oxides in different charge states.[7,20,21] It was predicted, that interstitial oxygen atoms tend to form the split interstitials (dumbbells) with regular oxygen ions in MgO[9,20,23] and α-Al_2O_3.[24-26] Similar split interstitials in the form of X^{2-} (X is halogen atom) called the H centers were studied experimentally in theoretically in alkali halides[27-31] and alkaline-earth metal fluorides[32,33]. In binary oxides, split interstitials were observed experimentally in pure and defective SrO[34,35] and MgO with cation vacancies.[36]

In our recent publications, the site symmetry approach has been applied for point defects in the crystalline lattices demonstrating its efficiency in the formation energy calculations, *e.g.*, for carbon substitutes in oxygen sites (C_O) of ZnO[37] and oxygen vacancies (V_O) of CeO_2[38]. In the case of substitutes or vacancies, the site symmetry is considered only for Wyckoff positions occupied in a host crystal. In the current study, we extend this approach to the interstitial defects. In this case, one needs to find the splitting of vacant Wyckoff positions in the host crystal. Indeed, the α-Al_2O_3 is considered as a case study. In fact, the scenario described can be applied to different defective binary oxides.

In oxygen interstitial modelling, it is common to start with the octahedral position having the highest site symmetry. In recent corundum calculations[25,39,40] tetrahedral positions were also considered. However, the hexagonal structure of corundum allows *four* possible interstitial positions. In this Communication, we analyse symmetry and properties of these four possible interstitial positions, corresponding to unoccupied by atoms Wyckoff positions of corundum space group $R\bar{3}c$. We consider also transformation of interstitial oxygen atom into split interstitial and analyse relevant charge, spin and local structure changes.

In present work α-Al_2O_3 crystals containing oxygen interstitials in different configurations have been calculated

[a] Institute of Chemistry, St. Petersburg State University, Petrodvorets, Russia
[b] Institute of Solid State Physics, University of Latvia, Riga, Latvia.
[c] Max Planck Institute for Solid State Research, Stuttgart, Germany.
* Corresponding author <r.evarestov@spbu.ru>

using a basis set of a linear combination of atomic orbitals (LCAO) with B3PW[41] hybrid exchange-correlation functional as implemented in CRYSTAL14 package.[42] We have used the all-electron basis set for atomic Gaussian-type basis functions of oxygen (constructed using pure *s*- and *d*- as well as hybrid *sp*-AOs in the form of 6*s*-2111*sp*-1*d* as described elsewhere[43]), and developed in ref. 44 for Al the effective core pseudopotential (ECP) with basis set functions of $3s^2 3p^1$ external shell.

Oxygen interstitial defect calculations have been performed using 2×2×1 conventional supercell consisting of 120+1 atoms. To provide a balanced summation in direct and reciprocal lattices, the reciprocal space integration has been performed by sampling the Brillouin zone with the 4×4×4 Monkhorst-Pack[45] mesh. Within the SCF procedure, the accuracies (tolerances) 7, 7, 7, 7, 14 have been chosen for calculations of Coulomb and exchange integrals. The SCF convergence threshold for the total electronic energy has been set to either 10^{-7} a.u., for geometry optimization calculations, or 10^{-9} a.u. for vibrational frequency calculations. The frozen phonon method (direct method) has been used for the calculation of vibrational frequencies.[46,47] Elastic properties have been calculated as first numerical derivatives of analytical energy gradients as implemented in the CRYSTAL code.[42] The effective charges on atoms have been estimated using Mulliken population analysis.[48]

The high accuracy of our calculations can be demonstrated through basic bulk properties of corundum (table *SI*1). As expected, the B3PW functional reproduces the lattice parameters and the band gap very well. Note that our band gap energy as calculated with the B3PW functional is only slightly smaller than that calculated in ref. 36 with the HSE functional and a mixing parameter of 32%. Also, the calculated phonon frequencies at the Γ-point of the Brillouin zone and the elastic properties are very well consistent with the experiments (table *SI*1).

The formation energies for oxygen interstitial atom (O_i) in different split Wyckoff positions[38,49] have been calculated from the relevant total energies using the equation:

$$E_{form}^{O_i} = E_{total}^{Al_2O_3(O_i)} - E_{total}^{Al_2O_3(perfect)} - {}^1/_2\, E_{total}^{O_2}, \qquad (1)$$

where $E_{total}^{Al_2O_3(O_i)}$ the total electronic energy of supercell with O_i, $E_{total}^{Al_2O_3(perfect)}$ the total electronic energy of perfect supercell, $E_{total}^{O_2}$ the total electronic energy of O_2 molecule. In this Communication, we present and compare two different approaches for finding ground-state equilibrium of oxygen interstitial in crystal lattice. First one is the calculation by freezing coordinates of oxygen interstitial atom (O_i) and fully optimising all other atoms. Then, the distance between O_i and the host oxygen atom (O_{reg}) changed in the initial configuration. In this way the O_i atom moves from the octahedral position towards the O_{reg} atom step by step. After each step O_i has been further displaced, in order to find lower energy states, and the procedure has been repeated. The second approach is based on the analysis of site symmetry and the Wyckoff positions splitting in the supercells.[38,49] (Analogous site symmetry analysis has been performed recently for C_O substitutes in wurtzite-structured ZnO crystal.[37]) When analysing all possible interstitial positions by symmetry, we can find those with free spatial parameters which allows us to get the lowest in energy configuration using automated optimization procedure and assuming no specific path (in our case, dumbbell).

The α-A_2O_3 (corundum) crystalline structure corresponds to the rhombohedral space group $R\bar{3}c$ (No. 167) with rhombohedral lattice containing two α-A_2O_3 formula units (10 atoms) *per* primitive unit cell. Al and O atoms occupy 4*c* (0 0 z) and 6*e* (x 0 ¼) Wyckoff positions with the site symmetry *S3* = C_3 and *S2* = C_2 and one free parameter, respectively, in the hexagonal setting. We use designation *SP* for the site symmetry point group, consisting of *P* point symmetry operations.

For the oxygen interstitial in corundum, any of the following four vacant Wyckoff positions in primitive unit cell 2*a* (0 0 ¼), 2*b* (0 0 0), 6*d* (½ 0 0) and 12*f* (x y z) could be used. The first three of them have no free parameters, while the fourth one is the three free-parameter position. The site symmetry of these vacant Wyckoff positions is described by point groups *S6* = D_3 (2*a*), *S6* = C_{3i} (2*b*), *S2* = C_i (6*d*), *S1* = C_1 (12*f*). Due to the undefined values of three free-parameters of Wyckoff position 12*f*, it will not be used in our O_i interstitial calculations. The interstitial atom can be placed in any of three remaining vacant Wyckoff positions (2a, 2b, or 6d) as initial positions. However, in the supercell model (SCM) the position with site symmetry *S1* appears also as the result of 2b Wyckoff position splitting with specific coordinates (x y z) (see our explanation below).

To model the defective crystal within the SCM approach, one starts from the primitive unit cell of a host crystal using the integer linear transformations of basic translation vectors of the host lattice.[50] Let $\boldsymbol{a}_i(\Gamma_1)$ (i = 1, 2, 3) be the basic translation vectors of the initial direct Bravais lattice of type Γ_1 while $\boldsymbol{A}_j(\Gamma_2)$ (j = 1, 2, 3) be the basic translation vectors of the new Bravais lattice of type Γ_2 with the same point symmetry but composed of supercells. Then

$$\boldsymbol{A}_j(\Gamma_2) = \sum_i l_{ji}(\Gamma_2\Gamma_1)\boldsymbol{a}_i(\Gamma_1) \qquad |\det l| = L, \qquad (2)$$

where $l_{ji}(\Gamma_2\ \Gamma_1)$ are integer elements of the matrix $l(\Gamma_2\ \Gamma_1)$ defining the transition from the lattice of type Γ_1 to the lattice of type Γ_2.

According to ref. 50, the smallest supercells for rhombohedral lattices correspond to the following transformation matrices:

$$\begin{pmatrix} 2 & 1 & 1 \\ 1 & 2 & 1 \\ 1 & 1 & 2 \end{pmatrix} \quad (3) \quad \text{and} \quad \begin{pmatrix} 2 & 1 & 0 \\ -1 & 1 & 0 \\ 1 & 1 & 1 \end{pmatrix} \quad (4)$$

Let *L* be the number of primitive unit cells in the supercell. *L* = 4 for matrix (3) and *L* = 3 for matrix (4). Matrix (3) transforms rhombohedral lattice to the rhombohedral one, whereas matrix (4) transforms rhombohedral lattice to the hexagonal one.

The interstitial oxygen atom in corundum was emplaced in ref. 25 in the Wyckoff positions 2*b* with the site symmetry *S6* = C_{3i} as well as 6*d* with the site symmetry *S2* = C_i with no free parameter (these two positions are called octahedral and tetrahedral). The supercell used here consists of 120 atoms and corresponds to *L* = 12 for transformation matrix

$$\begin{pmatrix} 4 & 2 & 0 \\ -2 & 2 & 0 \\ 1 & 1 & 1 \end{pmatrix}. \qquad (5)$$

The transformation matrix (5) with *L* = 12 corresponds to transformation (4) from initial rhombohedral lattice to the hexagonal matrix (*L* = 3) followed by the transformation (6) of the hexagonal lattice to hexagonal one

$$\begin{pmatrix} 2 & 0 & 0 \\ 0 & 2 & 0 \\ 0 & 0 & 1 \end{pmatrix}, \qquad (6)$$

which possesses *L* = 4.

Let us assume that in the SCM model, periodically repeated point defects are placed in the positions with the site symmetry *SP* corresponding to the interstitial or substituted atom as well as in vacancy. In the case when the perfect crystal has the symmetry of space group $G = T_a F$, the SCM of the defective crystal is described by a space group $G_d = T_A F_d$, where G_d, T_A and F_d are subgroups of *G*, T_A and *F*, respectively. In our case of oxygen interstitial in corundum, the Wyckoff position *S6* = C_{3i} (2*b*), *G* is described as $R\bar{3}c$, T_a is the translation group of the host crystal with rhombohedral lattice, while *F* corresponds to C_{6v}. The symmetry groups G_d, T_a and F_d of defective crystal are defined by the supercell choice and can be found, using the new computer tools and programs available at the Bilbao Crystallographic Server (BCS).[51]

Using CELSUB program of BCS server, one finds that the space group $G_d = T_A F_d$ is $P\bar{3}$ (No 147) with T_A defined by the matrix (4) and $F_d = C_{3i}$. This symmorphic space group corresponds to inserting of oxygen interstitial in the Wyckoff position 2*b* (*S6* = C_{3i}) of the host crystal non-symmorphic space group $G = R\bar{3}c$. The program WYCKSPLIT from the BCS has been used here, to find the splitting of Wyckoff position 2*b* for the group-subgroup chain 167 ($R\bar{3}c$) >147 ($P\bar{3}$):

2*b* (group 167) = 1*a* 1*b* 2*d* 2*d* 3*f* 3*e* 6*g* 6*g* (group 147) (7)

The program WYCKSETS from the BCS gives that 1*a*-1*b* and 3*e*-3*f* are equivalent Wyckoff positions in the space group 147. The point symmetry of the group 147 Wyckoff positions is the following:

*S*1(6*g*), *S*2(3*e*), *S*3(2*d*) and *S*6(1*a*).

When inserting interstitial atoms in these Wyckoff positions with different site symmetries (Fig. 1), we observe different defect configurations and different formation energies after the structure relaxation. As shown in table 2, these energies could differ a lot: 8.02 eV (6.15 eV in ref. 25) and 3.99 eV for high site symmetry C_{3i} (*S6*, octahedral position) and low site symmetry C_i (*S1*, dumbbell), respectively.[25]

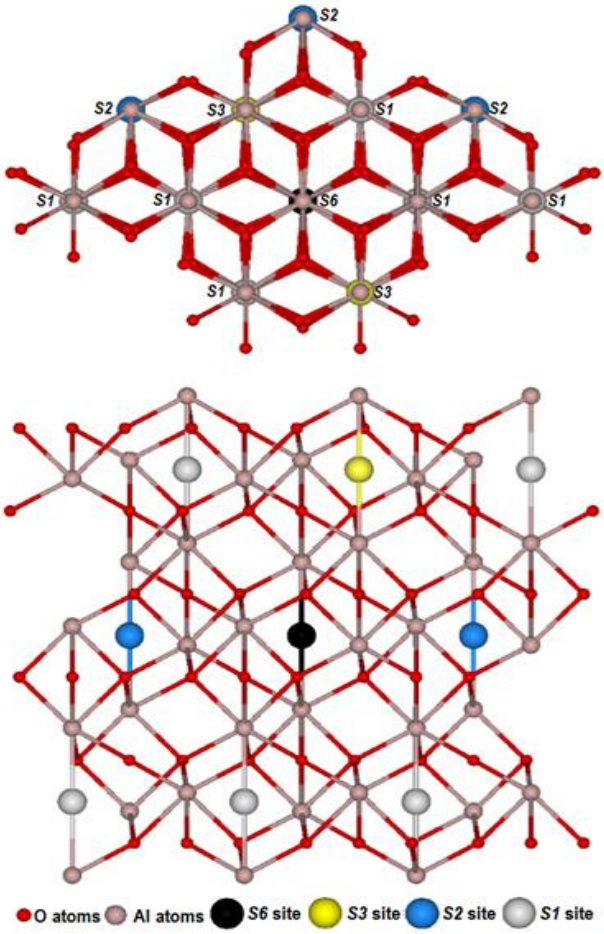

Figure 1 Atop (top) and aside (bottom) views of α-Al_2O_3 conventional supercell containing 120 atoms. The distribution of interstitials positions over 4 orbits is shown with different colours: *S*6 (black), *S*3 (yellow), *S*2 (blue), *S*1 (grey).

The difference of distances between interstitial and regular oxygens is also large 1.87 Å (2.17 in ref. 25) and 1.44 Å in octahedral and dumbbell configurations, respectively. Note that formation of the split oxygen interstitial in neutral supercell was demonstrated also in refs. 39, 40. Other authors considered doubly charged O_i in CeO_2 yet in order to obtain the O-O distance of 1.46 Å.[52] However, they did not perform group-theoretical analysis of host crystal Wyckoff position split in the SCM which we presented here. When making a supercell, a number of host crystal Wyckoff positions with different site symmetry appears. It leads to different possible population schemes for a single defect. This problem is not considered in the standard supercell simulations of defective crystals.

The results of hybrid B3PW calculations for four positions *S*1(6*g*), *S*2(3*e*), *S*3(2*d*) and *S*6(1*a*) are given in table 1 for closed shell (singlet) calculations. As one can see, the lowest formation energy (Eq. 1) 3.99 eV is obtained in our calculations for the lowest site symmetry *S1*. Such a configuration without symmetry operations corresponds to the split interstitial, called also the O_i-O_{reg} dumbbell (d = 1.44 Å) with preserved point symmetry of the oxygen site C_2. The dumbbell configuration is energetically more preferable, by 2.49 eV and 4.03 eV, than the configurations *S2* and *S3*, *S6*. In cases of higher symmetry (*S*6,

*S*3) the structure relaxation results in preserving octahedral surrounding of O_i, i.e. two Al and 6 O atoms at the distances 1.87 and 2.15 Å, and, consequently, highest formation energies (table 1). It is also reflected in very similar volume changes and very identical electronic density of states (DOS, fig. 2) for *S*3 and *S*6. The two positions differ only by the inversion operation, in contrast to less symmetric *S2*. For the tetrahedral *S*2 configuration, two nearest regular oxygen atoms are attracted to O_i (d = 1.86 Å) which leads to the volume increase by 0.12 Å^3 with respect to *S*3, *S*6. Two distinguishable DOS peaks at ~-2 and ~-6 (-4) eV below the Fermi energy are seen for *S*2 (*S*3, *S*6) in contrast to *S*1.

Table 1*. Closed shell (singlet) calculation results for O_i atom placed in four different split vacant positions.* The Wyckoff position (2b) of O_i is split into 4 orbits in the 120 atoms supercell: *a*, *d*, *e*, *g*. *SP* denotes the site symmetry group with *P* point group operations. 1NN and 2NN denote first and second nearest neighbours.

Position	*a* (*S*6)	*d* (*S*3)	*e* (*S*2)	*g* (*S*1)
Initial coordinates	0 0 0	1/3 -1/3 -1/6	½ 0 0	1/6 1/3 -1/3
Point group	C_{3i}	C_3	C_i	C_1
$E_{form}^{O_i}$, eV	8.02	8.02	6.48	3.99
1NN Distance d, Å	2 Al 1.87	2 Al 1.87	2 O 1.86	1 O 1.44
2NN Distance d, Å	6 O 2.15	6 O 2.15	2 Al 1.89	1 Al 1.85

*graphical images of these configurations are given in ESI (Figure *SI*1)

As demonstrated here, use of the free-parameter 6*g* position (*S1*, space group 147) split from initial 2*b* (Eq. 7) position (space group 167) in the SCM is sufficient to obtain the dumbbell configuration as a result of the automated structure optimisation making no assumption on the O_i path from the starting position.

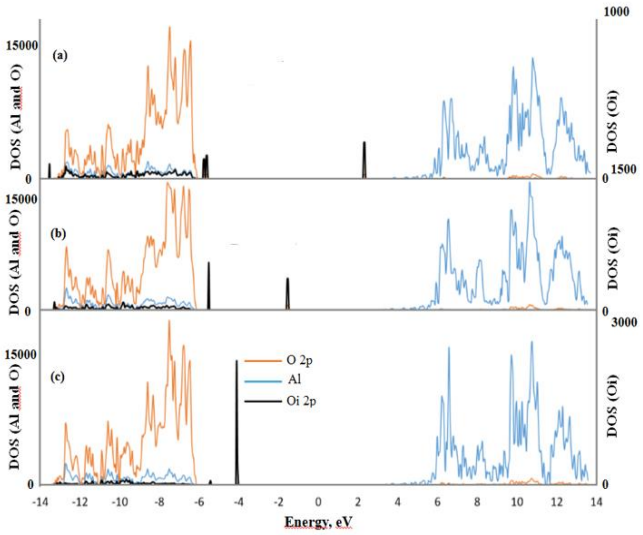

Fig. 2 Densities of states (DOSs), which are expressed in arbitrary units, obtained from calculations of *S1* (dumbbell) (a), *S2* (b) and *S3/S6* (c) O_i position. The dashed lines correspond to Fermi energy.

Analysis of the DOS (fig. 2) shows that this configuration leads to formation of occupied band in the band gap near the top of the valence band, and unoccupied states close to the conduction band bottom. Both oxygen atoms, *i.e.* O_i and O_{reg}, are equivalent and have identical charges (0.58 *e*), i.e. O_2^--superoxide ion, and each atom forms two bonds with aluminium atoms. The Mulliken population analysis does not show any bond population between O_i and O_{reg}.

It is worth mentioning that the site symmetry approach and group theoretical analysis as presented here allow analysis of the possible magnetic interstitial configurations. In general, the number of such configurations depends on the O_i position and its symmetry. However, one magnetic configuration is common for all the four positions considered split from initial 2*b* position (Eq. 7). This configuration with formation energy of 5.9 eV is characterized by a non-zero magnetic moment (μ) on seven oxygen atoms, with the largest μ on O_i (the so-called high symmetry triplet state) retaining the octahedral surrounding (table 2). In addition, we obtained two more solutions for the low symmetry triplet state with higher $E_{form}^{O_i}$ of 6.27 eV. In this case the magnetic moment is observed on 3 O atoms (including O_i), which is possible for *S*1, *S*2, *S*3 (table 2). The two low symmetry magnetic configurations are characterized by the same $E_{form}^{O_i}$ and distance between O_i and closest O_{reg} (1.89 Å). However, the distance between O_i and closest Al atom is different (1.85 and 2.02 Å). It should explain different spin distributions for the two low symmetry configurations, i.e. the larger μ of O_i in the case of shorter distance with Al.

We have also performed the vibrational frequency frozen phonon[46,47] calculations for the energetically most favourable dumbbell configuration, and compared the calculation results with available experimental and theoretical results for other O-O species (table 3). Unfortunately, the calculation of phonon frequencies for O_i is overlooked in the literature. However, it should give important information on its properties. The dumbbell configuration has the stretching O_i-O_{reg} vibrational mode with the frequency of 1067 cm^{-1} which is close to what observed typically for superoxide ions O_2^-. This frequency is well separated from other calculated frequencies which do not exceed 880 cm^{-1}. Notice that the calculated vibrational frequencies for the closed shell (singlet) solution *S*2 and *S*3 were imaginary, indicating their instability. On the other hand, the high symmetry triplet state for *S*3 did not show the presence of imaginary frequencies and thus, is a stable solution. There also exist a number of stretching and bending modes of different frequencies, respectively, 150, 557, 636 cm^{-1} and 271, 338, 350 cm^{-1} due to the interactions of O_i with the closest Al and O atoms in the octahedral position. On the basis of these results, we may conclude that the calculation of phonon frequencies is sensitive to the choice of interstitial configuration, first, and is necessary to discuss the nature of O-O defect fully, second. In fact, when the O_i atom leaves the octahedral site, it is in the triplet state, but after displacement by 0.5 Å, it turns out to be singlet, until it transforms into the dumbbell. This very small energy barrier explains why we do not observe imaginary vibrational frequencies for the triplet state.

Fig. 3 shows the results of closed shell (singlet) and open shell (triplet) calculations using our first approach as described above. As well seen, the two curves for the singlet and triplet solutions intercept at the distance from the

octahedral position of ~0.5 Å. which is equivalent to the O_i-O_{reg} distance of ~1.9 Å. So, the triplet state could be favourable at the distances larger than that value which is in agreement with our data in tables 2 and 3 and ref. 25.

Table 2*. Open shell (triplet) calculation results. μ the spin magnetic moment.

$E^{O_i}_{form}$, eV	5.91	6.27	6.27
1NN Distance d, Å	2 Al 1.91	O 1.89	2 Al 1.85 1.88
2NN Distance d, Å	6 O 2.14	Al 2.02	O 1.89
$\mu(O_i)$, μ_B	1.42	1.08	0.52
$\mu(O_{reg})$, μ_B	6 x 0.11	0.33 0.52	0.34 1.08

*graphical images of these configurations are given in ESI (Figure *SI*2)

Table 3.. Experimental and calculated properties of O-O species in different materials.

Material/ion	O-O bond length, Å		Frequency, cm^{-1}	
	Expt.	Calc.	Expt.	Calc.
α-Al_2O_3 (this work)		1.44		1067
O_2 [a, b]	1.208	1.22	1549	1550
Peroxide O_2^{2-} [c]	1.49	-	770	
O_i in CeO_2 [d]			2.26	
O_2^{2-} in CeO_2 (100) surface [e]		1.50		864 (100) surface
Superoxide O_2^- [c]	1.33		1090	
$Ni(O_2)$	-	1.382[f]	966[g]	982[f]
$(O_2)Ni(O_2)$[f]			1062	
O_2^- in $12CaO{\cdot}7Al_2O_3$ [h]	-	-	1131	-
O_2^- in $BaTiO_3$ [i]			1125	

[a] Ref. 53 [b] Ref. 54 [c] Ref. 55 [d] Ref. 52 [e] Ref. 56 [f] Ref. 57 [g] Ref. 58 [h] Ref. 59 [i] Ref. 60 * As demonstrated in Ref. 52 the ground state for O_i in CeO_2 has the distance between the two oxygen atoms 2.26 Å.

In conclusion, by means of the site symmetry analysis we have found and compared four possible spatial configurations for inserting O atoms into interstitial positions in the α-Al_2O_3 crystalline lattice. Counter-intuitively, the configuration highest by symmetry in the SCM has the highest insertion energy. The interstitials are unstable with respect to the almost barrier-less transformation into the split interstitial (dumbbell) with the energy gain of 2.5 eV. In other words, oxygen interstitial transport in α-Al_2O_3 is controlled by the dumbbell bond breaking and re-forming, which is important for the prediction of radiation properties of material. Oxygen atoms in these dumbbells have the distance 1.44 Å typical for peroxides O_2^{2-} (in agreement with ref. 25) but the vibrational frequency of 1067 cm^{-1} and charge -1 *e* close to a free superoxide O_2^-.

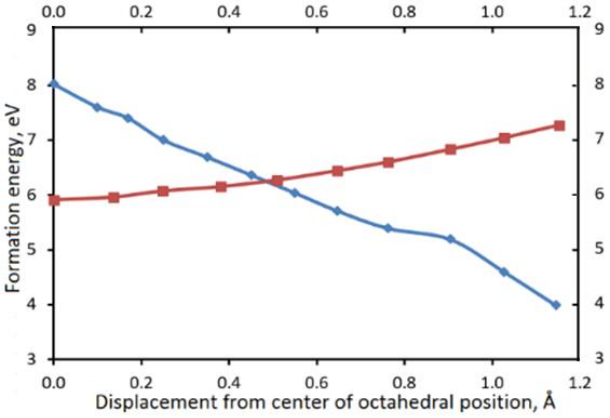

Fig. 3 The calculation results (formation energy as given by Eq. 1) due to frozen O_i coordinates (first approach). The O_i atom moved from the octahedral position (initial configuration) towards the O_{reg} atom forming the dumbbell defect (final configuration). Blue line (rhombs) corresponds to closed shell (singlet) whereas red line (squares) – to open shell (triplet) calculation.

Analysis of the DOS shows that the dumbbell produces the occupied states close to the valence band top and unoccupied states close to the conduction band bottom. The dumbbell optical absorption energy, 7-9 eV, falls into the UV region and hardly could be measured. Similar analysis could be performed for a wide class of defective crystalline materials. The lowest site symmetry group C_1 corresponds to dumbbell formation with the three free parameters and is therefore the most flexible in the defective crystal structure optimization. Of course, the site symmetry approach itself can be generalized to oxygen interstitials in other oxides, but, dumbbell configuration does not exist necessary in all oxides. The consideration the lowest symmetry C_1 sites only is not enough, as in many cases the lowest formation energy can correspond not only to C_1 symmetry, but also a higher one. As an example, we can mention Fe impurity in Ti site in $SrTiO_3$.[61] In fact, Fe impurity has tetragonal symmetry in this case, which agrees with the experimental data on absorption spectra. Meanwhile the formation energy for D_{4h} and C_1 symmetry is practically the same.

Acknowledgments

Authors are indebted to R. Vila, A. Popov and A. Lushchik for stimulating discussions. This work has been carried out within the framework of the EUROfusion Consortium and has received funding from the European Union's Horizon 2020 Research and Innovation Programme under grant agreement 633053. The views and opinions expressed herein do not necessarily reflect those of the European Commission. Support from Latvian National Research Program IMIS2 (2014–2017) is also appreciated. Calculations have been carried out using both the Marconi supercomputer system at Computational Simulation Centre and the Computer Center of St. Petersburg State University.

References

1 J.H. Crawford, *J. Nucl. Mater.*, 1982, **108**, 644-654.

2 J. Valbis and N. Itoh, *Radiation Eff. Def. Sol.,* 1991, **116**, 171-189.
3 F. Mota, C.J. Ortiz, R. Vila, N. Casal, A. Garcia, and A. Ibarra, *J. Nucl. Mater.,* 2013, **442**, Suppl. 1, S699-S704.
4 A. Serikov, L. Bertalot, M. Clough, U. Fischer, and A. Suarez, *Fusion Eng. Design*, 2015, **96-97**, 943-947.
5 P.W.M. Jacobs and E.A. Kotomin, *J. Am. Ceram. Soc.*, 1994, **77**, 2505–2508.
6 E.A Kotomin, A.I. Popov, and A. Stashans, *Phys. Status Sol. B*, 1998, **207**, 69-73.
7 E.A. Kotomin and A.I. Popov, *Nucl. Instr. Meth. B,* 1998, **141**, 1-15.
8 J.T. Devreese, V.M. Fomin, E.P. Pokatilov, E.A. Kotomin, R.I. Eglitis, and Yu.F. Zhukovskii, *Phys. Rev. B*, 2001, **63**, 184304.
9 P.W.M. Jacobs, E.A. Kotomin, and R.A. Evarestov, *Proc. SPIE*, 1997, **2967**, 153-158.
10 B.D. Evans, *J. Nucl. Mater.*, 1995, **219**, 202–223.
11 R.S. Averback, P. Ehrhart, A.I. Popov, and A. von Sambeek, *Rad. Eff. Def. Solids*, 1995, **136**, 169-173.
12 E.A. Kotomin, A.I. Popov, and A. Stashans, *J. Phys.: Cond. Matt.*, 1994, **6**, L569-L573.
13 A. Lushchik, Ch. Lushchik, K. Schwartz, F. Savikhin, E. Shablonin, A. Shugai, and E. Vasil'chenko, *Nucl. Instr. Meth. B*, 2012, **277**, 40–44.
14 J. Carrasco, N. Lopez, C. Souza, and F. Illas, *Phys. Rev. B*, 2005, **72**, 054109.
15 E. Feldbach, E. Tõldsepp, M. Kirm, A. Lushchik, K. Mizohata, and J. Räisänen, *Opt. Mater.*, 2016, **55**, 164-167.
16 A. Lushchik, Ch. Lushchik, K. Schwartz, E. Vasil'chenko, T. Karner, I. Kudryavtseva, V. Isakhanyan, and A. Shugai, *Nucl. Instr. Meth. B*, 2008, **266**, 2868-2871.
17 V.S. Kortov, V.A. Pustovarov, and T.V. Shtang, *J. Lumin.*, 2016, **169**, 24-28.
18 V.S. Kortov, V.A. Pustovarov, S.V. Zvonarev, and T.V. Shtang, *Rad. Meas.*, 2016, **90**, 90-93.
19 E.A. Kotomin, V.N. Kuzovkov, A.I. Popov, and R. Vila, *Nucl. Instr. Meth. B*, 2016, **374**, 107-110.
20 N.D.M. Hine, K. Frensch, W.M.C. Foulkes, and M.W. Finnis, *Phys. Rev. B*, 2009, **79**, 024112.
21 A. Platonenko, D. Gryaznov, S. Piskunov, Yu.F. Zhukovskii, and E.A. Kotomin, *Phys. Stat. Sol. C*, 2016, **13**, 932-936.
22 T. Brudevoll, E.A. Kotomin, and N.E. Christensen, *Phys. Rev. B*, 1996, **53**, 7731–7735.
23 R. A. Evarestov, P. W. M. Jacobs, and A. V. Leko, *Phys. Rev. B,* 1996, **54**, 8969-8972.
24 A. Platonenko, S. Piskunov, Yu.F. Zhukovskii, and E.A. Kotomin, *IOP Conf. Ser. Mater. Sci. Eng.*, 2015, **77**, 01200.
25 A.A. Sokol, A. Walsh, and C.R.A. Catlow, *Chem. Phys. Lett.*, 2010, **492**, 44-48.
26 Yu.F. Zhukovskii, A. Platonenko, S. Piskunov, and E.A. Kotomin, *Nucl. Instr. Meth. B*, 2016, **374**, 29-34.
27 A.L. Shluger, V.E. Puchin, T. Suzuki, K. Tanimura, and N. Itoh, *Phys. Rev. B*, 1995, **52**, 4017-4018.
28 K. Matsunaga, T. Tanaka, T. Yamamoto, and Y. Ikuhara, *Phys. Rev. B*, 2003, **68**, 085110.
29 J. Maeda and T. Okada, *J. Lumin.*, 2000, **87**, 564-567.
30 E.A. Kotomin, V.E. Puchin, and P.W.M. Jacobs, *Philos. Mag. A*, 1993, **68**, 1359–1367.
31 M.T.E. Halliday, W.P. Hess, and A.L. Shluger, *J. Phys.: Cond. Matt.*, 2015, **27**, 245501.
32 S. Parker, K.S Song, C.R.A. Catlow, and A.M. Stoneham, *J. Phys. C: Solid State Phys.*, 1981, **14**, 4009-4015.
33 F.U. Abuova, E.A. Kotomin, V.M. Lisitsyn, A.T. Akilbekov, and S. Piskunov, *Nucl. Instr. Meth. B*, 2014, **326**, 314–317.
34 V. Seman, S. Reifman, and T. Lehto, *Solid State Phys.*, 1980, **22**, 2244-2249.
35 V. Seman, S. Reifman, T. Lehto, and Ü. Haldre, *Phys. Stat. Sol. B*, 1980, **102**, 459.
36 A. Lushchik, T. Kärner, Ch.B. Lushchik, E. Vasil'chenko, S. Dolgov, V. Issahanyan, and P. Liblik, *Phys. Stat. Sol. C*, 2007, **4**, 1084-1087.
37 R.A. Evarestov, S. Piskunov, and Yu. F. Zhukovskii. *Chem. Phys. Lett.*, 2017, **682**, 91-95.
38 R.A. Evarestov, D. Gryaznov, M. Arrigoni, E.A. Kotomin, A. Chesnokov, and J. Maier, *Phys. Chem. Chem. Phys.*, 2017, **19**, 8340-8348.
39 M. Choi, A. Janotti, and C. G. Van de Walle, *J. Appl. Phys*., 2013, **113**, 044501.
40 M.Y. Yang, K. Kamiya, and K. Shiraishi, *AIP Advances*, 2013, **3**, 102113.
41 A.D. Becke, *J. Chem. Phys.*, 1993, **98**, 5648–5652.
42 R. Dovesi, V.R. Saunders, C. Roetti, R. Orlando, C.M. Zicovich-Wilson, F. Pascale, B. Civalleri, K. Doll, N.M. Harrison, I.J. Bush, Ph. D'Arco, M. Llunell, M. Causá, and Y. Noël, *CRYSTAL14 User's Manual* (University of Torino, 2014).
43 J. Baima, A. Erba, M. Rérat, R. Orlando, and R. Dovesi, *J. Phys. Chem. C* , 2013, **117**, 12864–12872.
44 M. Causá, R. Dovesi, and C. Roetti, *Phys. Rev. B*, 1991, **43**, 11937- 11943.
45 H.J. Monkhorst and J.D. Pack, *Phys. Rev. B*, 1976, **13**, 5188-5192.
46 F. Pascale, C.M. Zicovich-Wilson, F. Lopez, B. Civalleri, R. Orlando, and R. Dovesi, *J. Comput. Chem.*, 2004, **25**, 888-897.
47 C.M. Zicovich-Wilson, F. Pascale, C. Roetti, V.R. Saunders, R. Orlando, and R. Dovesi, *J. Comput. Chem.*, 2004, **25**, 1873-1881.
48 R.S. Mulliken, *J. Chem. Phys.*, 1955, **23**, 1833-1840.
49 R.A. Evarestov, Yu.E. Kitaev, and V.V. Porsev, *J. Appl. Crystal.*, 2017, **50**, 893-900.
50 R.A. Evarestov and V.P. Smirnov, *J. Phys.: Cond. Matt.*, 1997, **9**, 3023-3031.
51 http://www.cryst.ehu.es/.
52 P.R.L. Keating, D.O. Scanlon, and G.W. Watson, *Chem. Phys. Lett.*, 2014, **608**, 239-243.
53 CRC Handbook of Chemistry and Physics (74th Ed., edited by D.R. Lide, CRC Press, Boca-Raton, FL, 1993).
54 J. Rolfe, W. Holzer, W. F. Murphy, and H. J. Bernstein, *J. Chem. Phys.*, 1968, **49**, 963-975.
55 M. Hayyan, M.A. Hashim, and I.M. AlNashef, *Chem. Rev.*, 2016, **116**, 3029-3085.
56 T. Zacherle, A. Schriever, R. A. De Souza, and M. Martin, *Phys. Rev. B*, 2013, **87**, 134104.
57 C.J. Cramer, W.B. Tolman, K.H. Theopold, and A.L. Rheingold, *PNAS*, 2003, **100**, 3635-3640.
58 H. Huber and G.A. Ozin, *Can. J. Chem.*, 1972, **50**, 3746-3747.
59 K. Kajihara, S. Matsuishi, K. Hayashi, M. Hirano, and H. Hosono, *J. Phys. Chem. C*, 2007, **111**, 14855-14861.
60 P. Ren, N. Maso, and A.R. West, *Phys. Chem. Chem. Phys.*, 2013, **15**, 20943-20950.
61 R. A. Evarestov, S. Piskunov, E. A. Kotomin, and G. Borstel, *Phys. Rev B*, 2003, **67(6)**, 064101.

Institute of Solid State Physics, University of Latvia as the Center of Excellence has received funding from the European Union's Horizon 2020 Framework Programme H2020-WIDESPREAD-01-2016-2017-TeamingPhase2 under grant agreement No. 739508, project CAMART²

